Formation of amorphous iron-calcium phosphate with high stability

Song Chen[1#*], *Dachuan Liu*[1#], *Le Fu*[2#], *Bing Ni*[3], *Zongkun Chen*[3], *Jennifer Knaus*[3], *Elena V. Sturm*[3,4], *Bohan Wang*[2], *Håvard Jostein Haugen*[5], *Hongji Yan*[6,7,8], *Helmut Cölfen*[3*], *Bin Li*[1*]

[1] Orthopedic Institute, Department of Orthopaedic Surgery, The First Affiliated Hospital, School of Biology & Basic Medical Sciences, Suzhou Medical College, Soochow University, Suzhou, Jiangsu, China

[2] School of Materials Science and Engineering, Central South University, Changsha, China

[3] Physical Chemistry, Department of Chemistry, University of Konstanz, Universitätsstraße 10, 78457 Konstanz, Germany

[4] Section Crystallography, Department of Geo- and Environmental Sciences, Ludwigs-Maximilians-University Munich, Theresienstr. 41, 80333 Munich, Germany

[5] Department of Biomaterials, Institute for Clinical Dentistry, University of Oslo, PO Box 1109 Blindern, Oslo 0376, Norway

[6] Department of Medical Cell Biology, Uppsala University, Uppsala, Sweden

[7] AIMES - Center for the Advancement of Integrated Medical and Engineering Sciences at Karolinska Institutet and KTH Royal Institute of Technology, 171 77, Stockholm, Sweden

[8] Department of Neuroscience, Karolinska Institutet, 171 77, Stockholm, Sweden

These authors contributed equally to this work.

This article has been accepted for publication and undergone full peer review but has not been through the copyediting, typesetting, pagination and proofreading process, which may lead to differences between this version and the Version of Record. Please cite this article as doi: 10.1002/adma.202301422.

* Corresponding authors: Bin Li (binli@suda.edu.cn); Helmut Cölfen (helmut.coelfen@uni-konstanz.de); Song Chen (chensong@suda.edu.cn).

Keywords: biomineralization, amorphous calcium phosphate, ammonium iron citrate, phase transformation

Abstract

Amorphous iron-calcium phosphate (Fe-ACP) plays a vital role in the mechanical properties of teeth of some rodents, which are very hard, but its formation process and synthetic route remain unknown. Here, we report the synthesis and characterization of an iron-bearing amorphous calcium phosphate in the presence of ammonium iron citrate (AIC). The iron is distributed homogeneously on the nanometer scale in the resulting particles. The prepared Fe-ACP particles can be highly stable in aqueous media, including water, simulated body fluid and acetate buffer solution (pH 4). In vitro study demonstrates that these particles have good biocompatibility and osteogenic properties. Subsequently, Spark Plasma Sintering (SPS) is utilized to consolidate the initial Fe-ACP powders. The results show that the hardness of the ceramics increases with the increase of iron content, but an excess of iron leads to a rapid decline in hardness. Calcium iron phosphate ceramics with a hardness of 4 GPa can be achieved, which is higher than that of human enamel. Furthermore, the ceramics composed of iron-calcium phosphates showed enhanced acid resistance. This study provides a novel route to prepare Fe-ACP, and presents the potential role of Fe-ACP in biomineralization and as starting material to fabricate acid-resistant high-performance bioceramics.

1. Introduction

Calcium phosphates (CaPs) are the main inorganic components of vertebrate hard tissues. Amorphous calcium phosphate (ACP), prevalent in biological organisms, represents a unique class of calcium phosphates[1]. It has no translational and orientational long-range order of the atomic positions, showing essentially glass-like physical properties[2]. Previous studies revealed that

intracellular ACP precursors reside in the mitochondria of mineralizing cells, and they are transferred from mitochondria via the lysosomal pathway[3]. Recent studies have suggested that ACP might be the precursor of many biominerals, and it plays a vital role in the functions of these structures[4]. As a transitory phase, ACP is highly unstable in an aqueous medium, readily transforming to crystalline calcium phosphates such as hydroxyapatite[5]. Some trace elements such as magnesium and strontium have been found in natural hard tissues, and these divalent ions are able to stabilize ACP by either substituting the calcium or adsorbing on the surface of ACP to disrupt the crystallization process [6]. Recently, the function of iron-based phases in the biomineralization process has attracted much attention. Iron has been found to exist in hard tissues of organisms in various forms, such as ferrihydrite, magnetite and goethite[7]. The function of iron oxide in teeth hardening has been demonstrated in limpets, chitons and chichlid fishes [8]. Another study shows that the iron-rich phases strengthen the incisor of feral coypu. The iron-rich enamel shows a higher mechanical strength (Hardness ~ 4.6 GPa) than the nonpigmented enamel (Hardness ~ 3.5 GPa)[9]. Moreover, a recent investigation on rodent teeth shows that amorphous intergranular phases control the mechanical properties of enamel. The mixture of ferrihydrite and amorphous iron-calcium phosphate in the intergranular phases makes the enamel harder and more resistant to acid attack[10]. An important question related to iron-hardened minerals is how iron-rich phases such as amorphous iron-calcium phosphate (Fe-ACP) are formed. Previous studies have shown that the presence of iron affects the crystallinity and solubility of hydroxyapatite and octacalcium phosphate[11]. However, there is still no evidence revealing the mechanisms of formation of the Fe-ACP in aqueous media, whether or not such an iron-bearing amorphous phase is a transient precursor remains unclear. Therefore, the synthesis of Fe-ACP and the unrevealing of its formation process are essential for understanding biomineralization of iron-rich calcium phosphate-based biominerals.

Except for the important role of biomineralization, iron-based materials show great potential in the biomedical field. As an essential component for cell metabolism and biochemical reaction, iron plays a crucial role in some body functions such as oxygen transport, DNA synthesis and cooperates with many enzymes. Iron-containing particles have been successfully applied in photothermal and photodynamic therapies for the treatment of cancer [12]. More recently, the function of iron-based bioceramics in tissue regeneration has been extensively explored. It is found that iron-containing

bioceramics can promote angiogenesis and osteogenesis by regulating the expression of vascular endothelial growth factor and HIF-1α in endothelial cells [13]. Our recent research has shown the great osteogenic property of an iron-bearing calcium phosphate cement in vivo[14]. The use of amorphous calcium phosphate in the biomedical field has been reported, including implant coatings[15], drug delivery vehicles [16] and reinforcing agents for self-setting cements[17]. Therefore, it is our interest to synthesize the iron-containing ACP particles and explore their potential use in the dental and orthopedic fields.

Many attempts have been made to produce ACP using wet route syntheses or dry route syntheses[18]. The wet synthesis route usually involves the rapid mixing of calcium salt with phosphate salt to prevent phase transformation during the preparation. Organic molecules such as polyacrylic acid (PAA)[19], polyaspartic acid (PASP)[20], polyethylene glycol[18a], poly(allyamine) hydrochloride[21] and triethylamine[22] have been applied to slow down the conversion rate. Citrate ions, which account for 1-2 wt % of natural bone, significantly affect the stability of calcium phosphates and regulate their crystal growth[23]. It is worth noting that most reported ACP are prepared under neutral or basic conditions, and the study by Posner has shown that increasing pH can greatly slow down the conversion rate of ACP[24]. At a more acidic pH, dicalcium phosphate dihydrates and octacalcium phosphates are the most common phases. In the presence of magnesium and citrate ions, which are known as crystallization inhibitor of apatite, acidic ACP can be prepared at solution pH of 6.0-6.5 [25]. Although an acidic disordered form of calcium phosphate is detected in the bones of zebrafish[26], to the best of our knowledge, no ACP has been prepared in even more acidic aqueous solutions. In the oral environment, the acidic ACP-containing materials can take advantage of enhanced acid-resistance, which can potentially be applied as dental repair materials. Moreover, when preparing the iron-bearing calcium phosphates, the acidic reaction medium can minimize the precipitation of iron hydroxide, which might facilitate the formation of Fe-ACP.

In the present work, we have explored the synthesis routes to prepare an iron-bearing amorphous calcium phosphate in aqueous media at ambient temperature. Ammonium iron citrate (AIC), which contains both iron and citrates, is selected as the iron source for the preparation. The amorphous iron-calcium phosphate can be prepared at pH values as low as 4 prepared in the presence of AIC. The resultant particles kept their amorphous feature in water and SBF solution when prepared

under high concentration of AIC. The iron-containing calcium phosphate particles showed good biocompatibility and osteogenic properties in vitro. Subsequently, the synthesized Fe-ACP was applied as starting material to fabricate acid-resistant high-performance bioceramics. Together, the study reveals clues about the biomineralization process of Fe-ACP and provides new insight into the stability of the amorphous phase. The as-synthesized particles might play a key role in the biomineralization process of iron-rich hard tissues, and possess potential as starting materials to fabricate acid-resistant high-performance bioceramics.

2. Results and discussions

2.1. Preparation and characterization of Fe-ACP

Typical Fe-ACP particles which were synthesized with 0.3 M PO_4^{3-}, 0.5 M Ca^{2+} and 0.04 M ammonium iron (III) citrate (the pH after reaction is around 5 without adjustment) is shown in **Figure 1.** The diameters of the particles are between 50 nm and 200 nm (**Figure 1**a). TEM and SAED pattern confirmed that the prepared particles were non-crystalline nanoparticles (**Figure.1**b, c). The specimen exhibited peaks of Fe 2p, O 1s, Ca 2p, C 1s, and P 2p over a wide binding energy region (**Figure 1**d). The binding energy of the Fe $2p_{3/2}$ peak was 710 eV (**Figure 1**e), which can be assigned to Fe^{3+} bonded to phosphate groups [27].

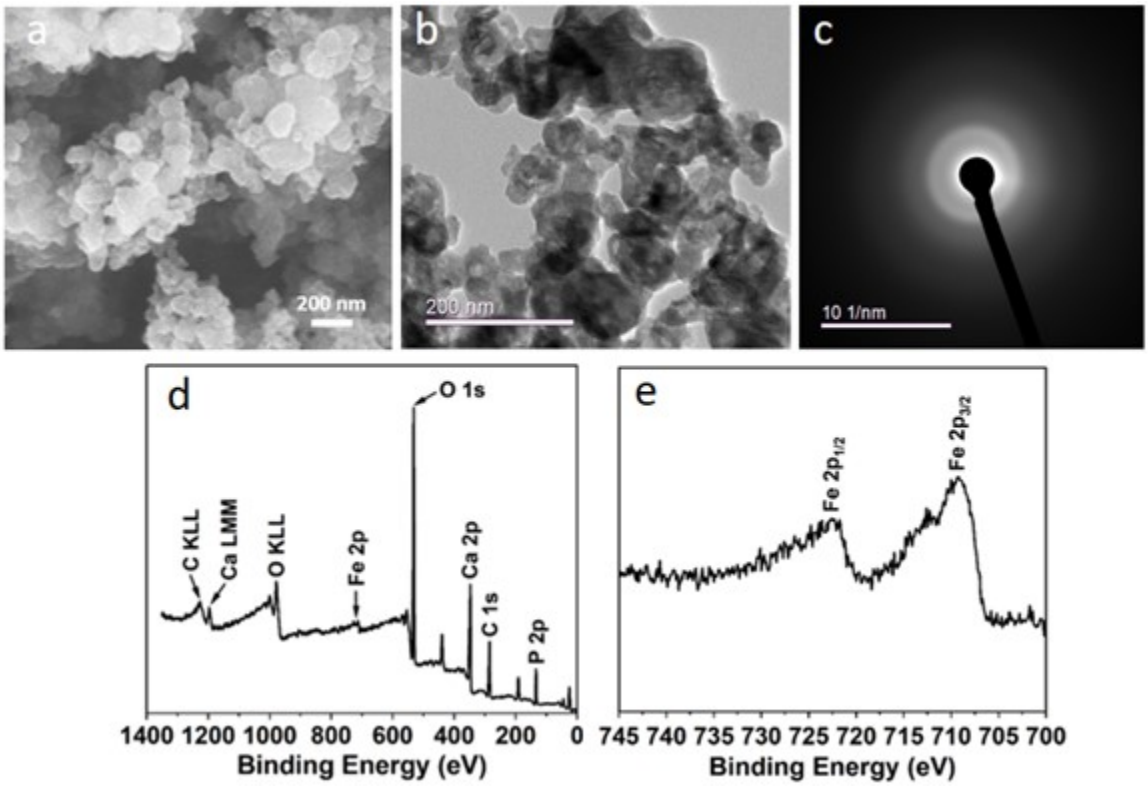

Figure 1. Typical amorphous iron-calcium phosphate prepared in the presence of 0.04 M ammonium iron (III) citrate. (a) SEM image (Magnification x50 000). (b) TEM micrograph (Magnification x40 000). (c) SAED pattern of the particles. (d) The XPS spectra over a wide range. (e) The XPS spectra of the Fe $2p_{3/2}$ peak.

We have shown that the concentration of ammonium iron citrate is essential for forming Fe-ACP. (**Figure 2**). The preparation of amorphous calcium phosphate by precipitation is usually conducted in alkaline solutions [28]. Under acidic conditions, the final products are normally brushite (dicalcium phosphate dihydrate, $CaHPO_4{\cdot}2H_2O$, DCPD) or monetite (dibasic calcium phosphate anhydrate, $CaHPO_4{\cdot}2H_2O$, DCPA) with high crystallinity [29]. Although ACP has been prepared at pH 6 in the presence of magnesium and citrate ions, the synthesis of ACP at pH lower than 5 has, to our knowledge, never been reported. Our previous research showed that cetyltrimethylammonium bromide and ammonium chloride effectively regulate the crystal growth of CaPs, forming DCPD or

DCPA particles with various morphologies and hierarchical structures[30]. In this study, we have shown that AIC is a strong crystallization inhibitor of acidic calcium phosphates, with which ACP under pH 5 was synthesized. As shown in **Figure 2**, the inhibition effect of AIC is concentration-dependent. With a low concentration of AIC (0.007 M and 0.02 M), the final phase was still brushite (**Figure 2**a), but the morphology of the powders changed from micro-sized platelets to block-like particles (**Figure 2**c). Nano-sized Fe-ACP can be obtained by increasing the AIC concentration up to 0.04 M. Further increasing the AIC concentration to 0.1 M and 0.2 M had no influence on the morphology and final phase of the particles. We further investigated the inhibition effects of citrate and iron ions respectively to better understand the formation process of Fe-ACP. The presence of iron ions alone was not effective in forming the Fe-ACP (Figure S1). With 0.04 M or 0.10 M iron nitrate, the crystalline phase was still plate-like brushite. Previous studies revealed that citrate regulates the crystal growth of hydroxyapatite by strongly binding to the hydroxyapatite surface[31]. More recently, it is found that the citrates can facilitate the intrafibrillar formation of hydroxyapatite to produce an inorganic-organic composite by reducing the interfacial energy between the biological matrix and the amorphous calcium phosphate precursor[32]. In accordance with these reports, hydroxyapatite nanocrystals formed in the presence of citrate (Figure S1a and b). Therefore, the formation of Fe-ACP is regulated by the synergistic effect of both iron ions and citrates.

The structural differences of the obtained particles were confirmed by infrared spectra (**Figure 2**b). The spectrum showed sharp bands of $v_2PO_4^{3-}$ (~985 cm^{-1}), $v_3PO_4^{3-}$ (~1056 cm^{-1} and ~1132 cm^{-1}) and $v_4PO_4^{3-}$ (~524 cm^{-1}). In contrast, the spectra of AIC004, AIC010, and AIC020 had rounded absorption bands around 556 cm^{-1} and 1074 cm^{-1}, confirming the amorphous features of these samples [28, 33]. It is worth noting that particles prepared in the presence of AIC show additional bands around 1400 cm^{-1} and 1610 cm^{-1}, which can be attributed to vibrations of the carboxyl group for the associated citrate, suggesting a relevant amount of citrate remaining in the resultant particles [31c, 34].

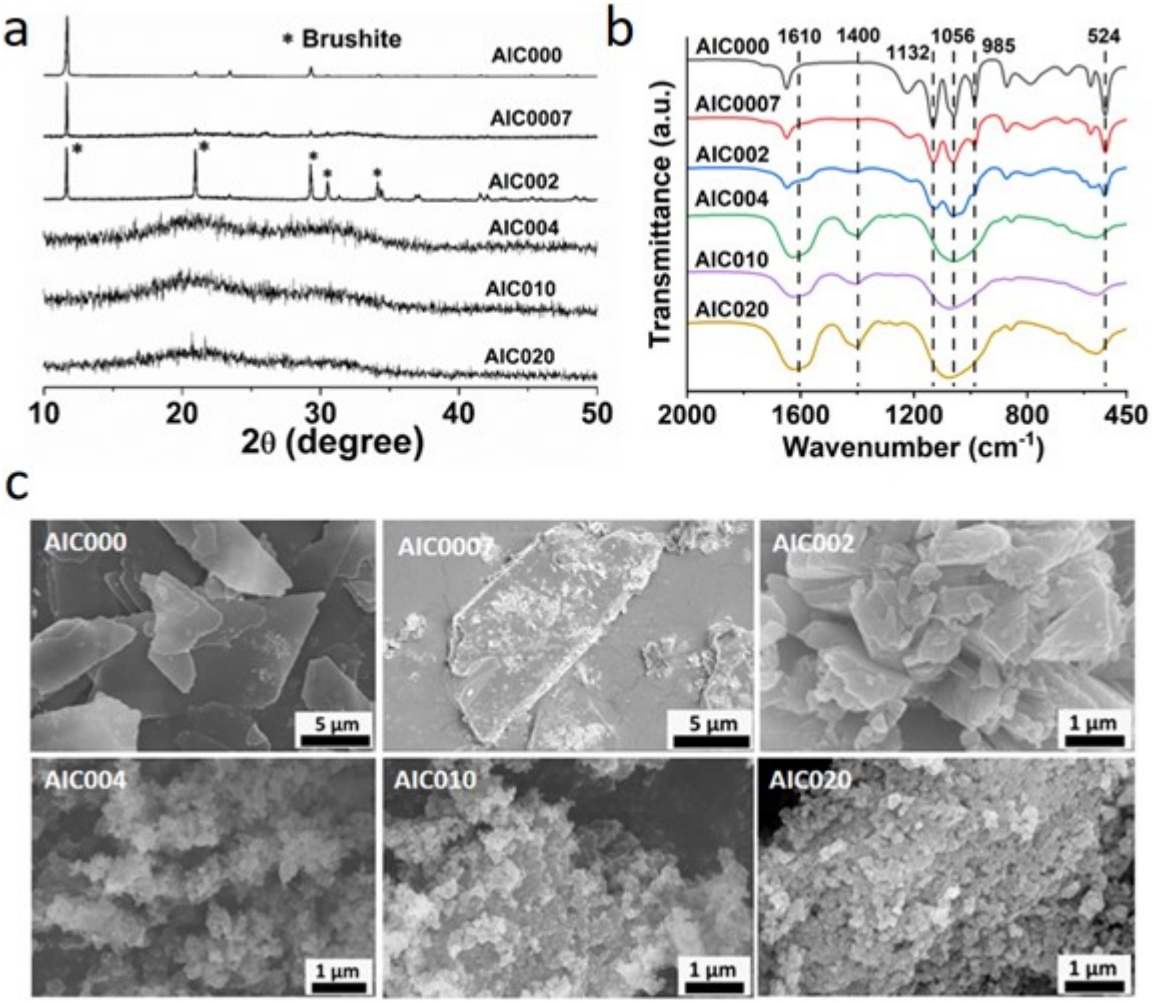

Figure 2. Effect of AIC concentration on the preparation of the particles. (a) XRD of the powders prepared at different concentrations of AIC. The patterns are matched with the standard diffraction pattern of brushite (PDF 01-072-0713). (b) FTIR of the powder. (c) SEM of the particles (Magnifications x5 000 and x20 000).

The pH changes during the synthesis of AIC000, AIC004, AIC010 and AIC020 are shown in **Figure S**2. The final pH dropped with the addition of 0.04 mol/L AIC, but continuously increasing the AIC concentration in the solution to 0.10 mol/L and 0.20 mol/L resulted in a slight increase in the pH. The chemical composition of Fe-ACP is reported in **Table S**1. TGA-DTG analysis revealed that all the

samples present a small amount of carbonate and citrate ions (**Figure S**3). In general, the amount of iron, as well as citrate and carbonate in the particles, increased with the AIC concentration in solution. The detected Fe/(Ca+Fe) ratio was 0.11 when the concentration of AIC was 0.07 mol/L, and it increased to 0.29 and 0.35 when 0.10 and 0.20 mol/L AIC were added. Simultaneously, the amount of phosphate decreased with increasing AIC concentration. Possibly, it was replaced by carbonate and citrate. The structural water content for AIC 0007 was around 5.0 % and it increased to 8.7% for AIC020 samples. The percentage of adsorbed water varied in the range of 16-21%. It is worth noting that Fe-ACP can be prepared even at pH 4 (adjust with hydrochloric acid) at the presence of 0.10 mol/L AIC (**Figure S**4). The resulting particles were spherical, with diameters around 300 nm. The Fe/Ca ratio of the particles was higher than that of the particles prepared at pH 5. TEM images showed that some kind of layered structure existed within the AIC004 particles (**Figure 3**a), which was not observed in AIC010 particles (**Figure S**5a). The element mapping showed that the iron was uniformly distributed among the particles (**Figure 3**b-c, and **Figure S**5b-c).

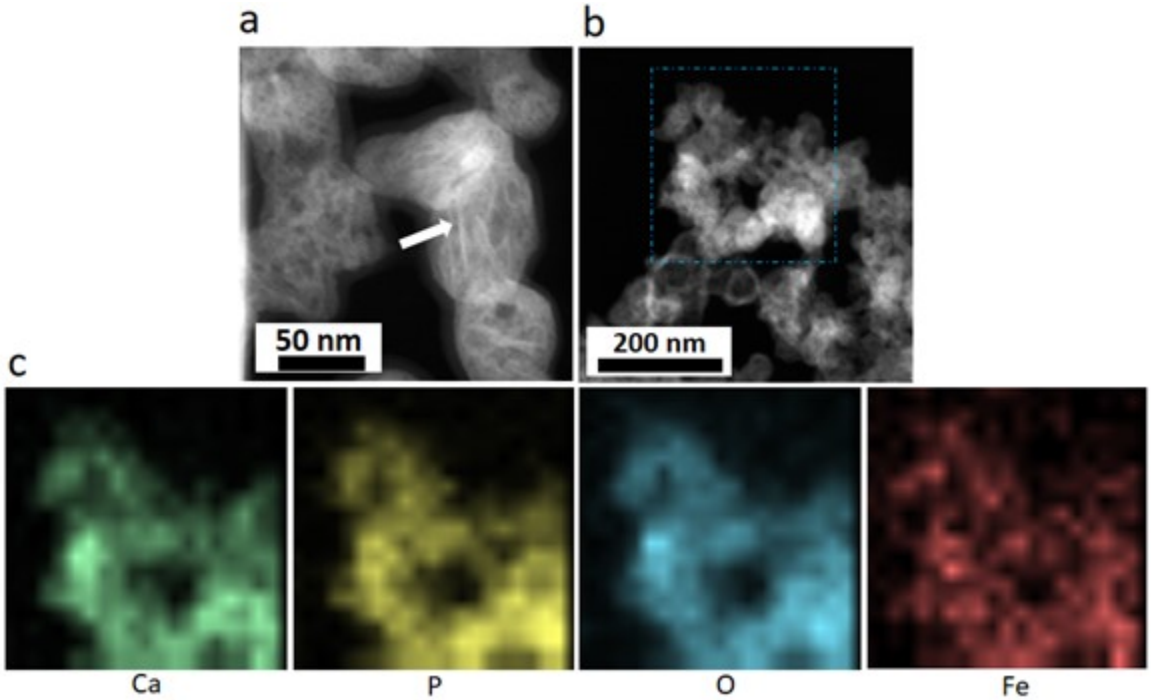

Figure 3. High-angle annular-dark-field (HAADF) scanning TEM images of particles prepared with 0.04 M AIC (Magnification x800 000). (a) Image showing the layered structure within the particles. (b) and (c) EDX mapping of the particles.

2.2. Stability of Fe-ACP

In the bone mineralization process, ACP has been proposed as the precursor and transition phase of crystalline apatite[4c, 5b, 35]. Several studies have investigated the phase transformation process of ACP to crystalline calcium phosphates in solution[36]. In an aqueous solution, the amorphous phase can only exist for several hours[37]. The conversion rate can be slowed down by adding stabilizers such as polyethylene glycol[38] or adenosine triphosphate[39]. Some ions such as magnesium and strontium are demonstrated to be efficient in stabilizing the ACP as well[6b, 40]. In this study, the stability of Fe-ACP was investigated by immersing the particles in water and simulate body fluid (SBF, the composition is shown in the Materials and Methods section). It is interesting to find that the stability of these particles is highly related to the concentration of AIC used during preparation. AIC004 (0.04 mol/L AIC) particles transformed to hydroxyapatite after immersion in water and SBF for 7 days (**Figure 4** a, b). The particles after conversion showed irregular plate-like morphology (**Figure S**6). When the concentration of AIC was 0.10 mol/L (AIC010), no conversion was observed, even after 31 days of immersion in water and SBF (**Figure 4** a and b). This was further confirmed by TEM micrographs and SAED patterns of AIC010 particles, which have shown amorphous features after immersion in SBF for 7 days and 31 days (**Figure S**7). It is similar for AIC020 particles, which showed no phase transformation after storage for 45 days in water and SBF (**Figure S**8). This can likely be attributed to the inhibiting action of citrate, which is known to stabilize ACP[41] and even prenucleation clusters as well as liquid precursor phases[42]. That way, crystallization can be effectively inhibited. We further investigated the thermal stability of the AIC particles by TGA/XRD. As shown in **Figure 4** c, continuous weight loss is observed on heating Fe-ACP. The water molecules loosely absorbed on the surface of Fe-ACP were removed between 25 ºC and 200 ºC. The weight loss in the range of 200 ºC and 400 ºC was attributed to the loss of strongly bound water molecules. The total mass loss up to 800 ºC was around 25%. The XRD patterns showed that the particles kept their amorphous feature when heating up to 500 ºC, without any diffraction peaks. At 800 ºC, the amorphous phase converted to calcium iron phosphate ($Ca_9Fe(PO_4)_7$) (**Figure 4** d). Dissolution experiments were carried out in acetate buffer solution (pH 4,

the composition is shown in the Materials and Methods section) up to 15 and 60 minutes (**Figure 4** e and f, **Figure S**9). The AIC000, AIC004 and AIC010 sample showed similar Ca and P release, however, the amount of Ca and P in the acid buffer solution was lowest for AIC010-pH4 sample, indicating the highest stability against dissolution in an acetate buffer solution (**Figure 4** e and f).

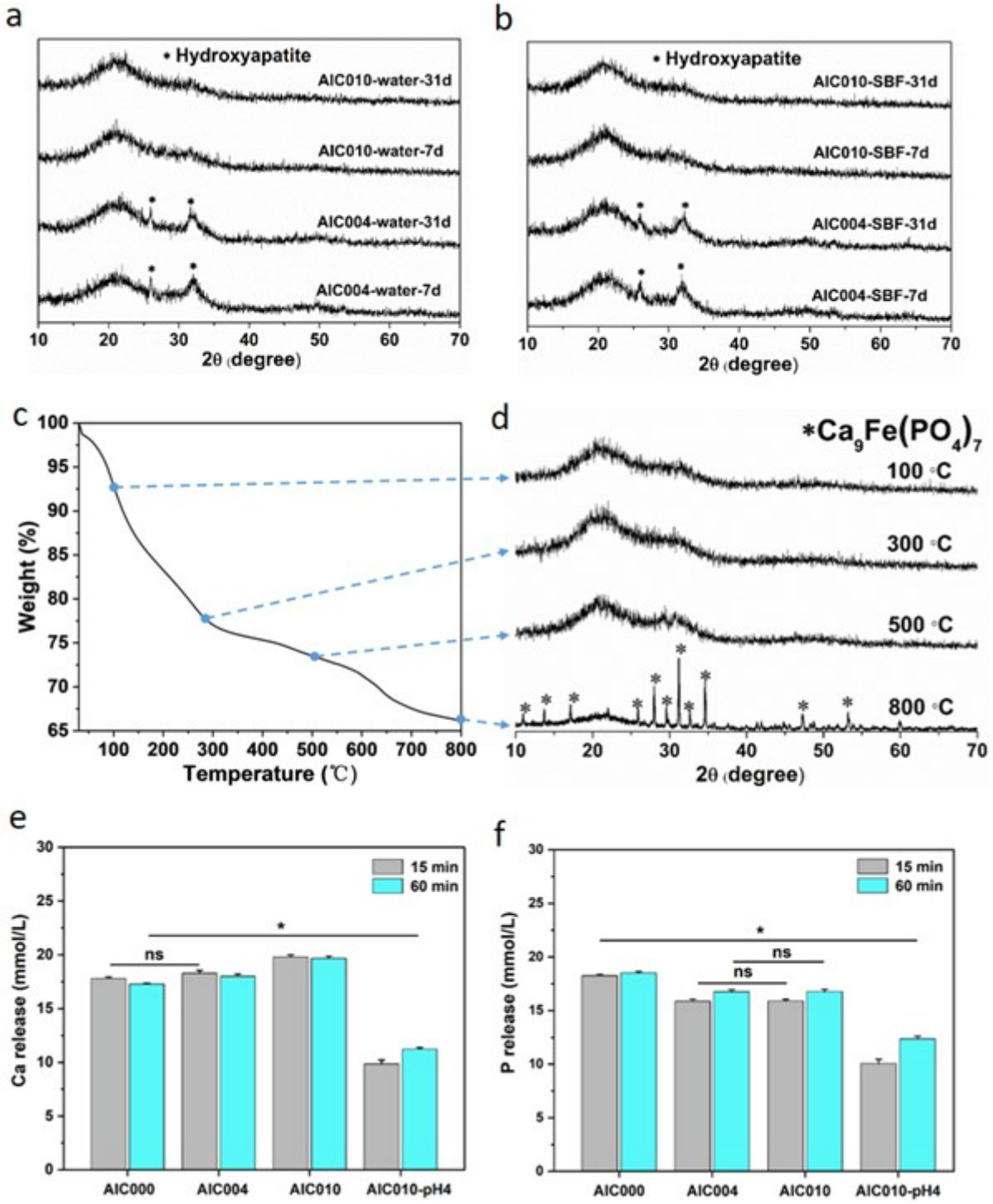

Figure 4. Stability of the Fe-ACP powder. (a-b) After storage for 7d and 31d in water (a) and SBF (b). (c) TGA curve of the AIC010 particles. (d) XRD of the particles heated to various temperatures. The

patterns are matched with the standard diffraction patterns of $Ca_{10}(PO_4)_6(OH)_2$ (PDF 00-001-1008) and $Ca_9Fe(PO_4)_7$ (PDF 01-089-0514) (e-f) The dissolution of the particles after exposure in the acetate buffer solution for 15 and 60 minutes (n=4).

2.3 Biological performance of Fe-ACP

Calcium phosphate-based materials show good biocompatibility and bioactivity, having broad applications in dental and orthopedic fields[43]. As one of the trace elements in the human body, an iron ion is non-toxic in a physiological range[44]. In order to verify the biocompatibility of Fe-ACP nanoparticles, the effects of Fe-ACP nanoparticles with different concentrations and iron contents on cell proliferation activity were investigated. Fe-ACP nanoparticles had no inhibitory effect on cell proliferation at the concentrations of 50 μg/ml, 100 μg/ml, and 200 μg/ml (Figure 5a-c). With higher concentrations of Fe-ACP particles (100 μg/ml and 200 μg/ml), the cell proliferations were slightly promoted. Alkaline phosphatase staining (ALP) and alizarin red staining (ARS) were applied to evaluate the osteogenic properties of AIC010 nanoparticles (Figure 5d and e). The ALP activity of bone marrow mesenchymal stem cells (BMSCs) at 7 days was significantly enhanced by AIC010 particles, and the promotion effect increased with the increase of concentration (Figure 5d). At 14 days, the BMSCs cultured with AIC010 particles showed more matrix mineralization (Figure 5e). The in vitro study revealed that the Fe-ACP particles had good biocompatibility and osteogenic properties, having the potential to be applied in the biomedical field.

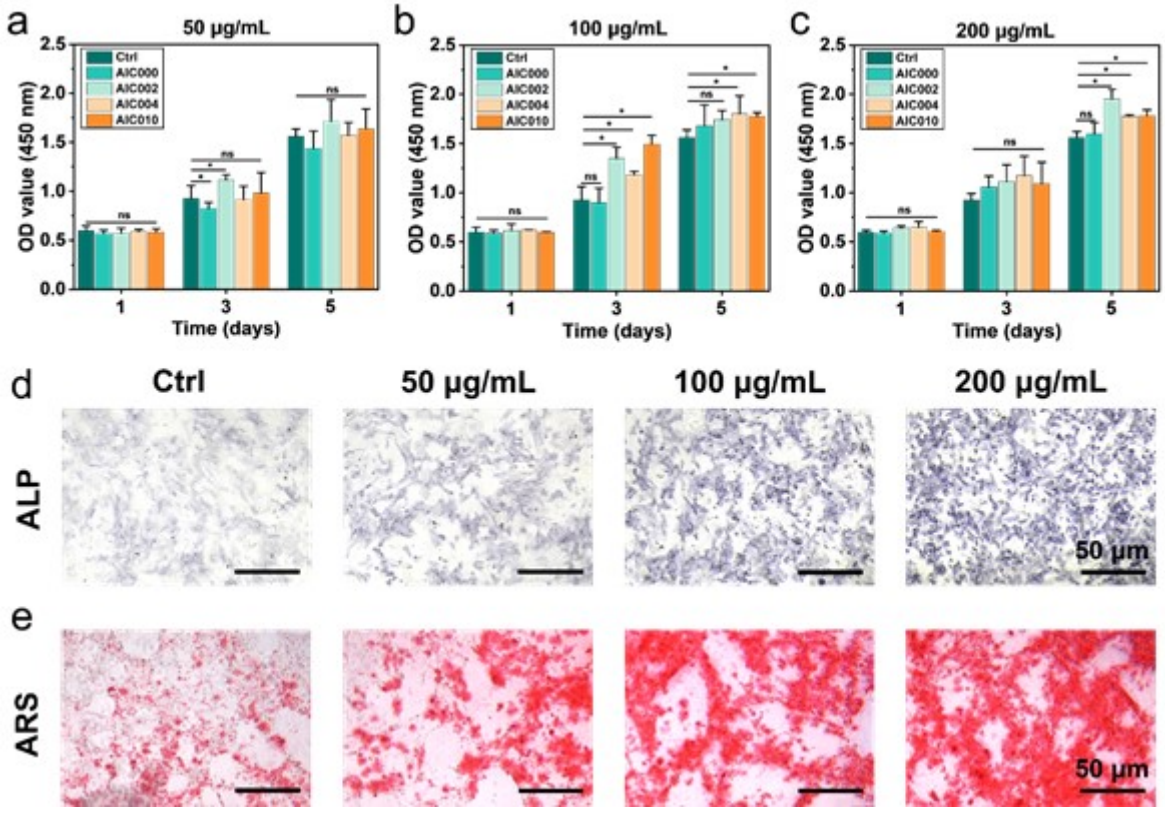

Figure 5. The proliferation of BMSCs cultured with different concentrations of Fe-ACP nanoparticles (a) 50 μg/mL, (b) 100 μg/mL, (c) 200 μg/mL was detected by CCK-8 assay at days 1, 3, and 5 (n=6). (d) ALP staining images of BMSCs cultured for 7 days with different AIC010 particles. (e) Alizarin red staining images of mineralized BMSCs cultured with AIC010 particles for 14 days.

2.4. Spark plasma sintered bioceramics

One potential application of the Fe-ACP particles is as starting materials for high-performance bioceramics. In this study, Spark Plasma Sintering (SPS) was used to sinter calcium iron phosphate ceramics. Our results have clearly shown that the presence of iron has a great impact on hardness of sintered bioceramics. The ceramics without iron showed a hardness of 3.0 GPa, and it reached 4.0 GPa for the AIC010 sample, which is higher than that of human enamel (~2.7 GPa-3.7 GPa)[45]. Further increasing the iron content (AIC020) resulted in a decrease in hardness (2.3 GPa) (**Figure 6**a). This is in accordance with the findings in rodent teeth, showing that the iron-containing enamel is harder than that without iron[10]. XRD patterns of the sintered ceramics are shown in **Figure 6**b. The final phase of

the ceramics was $Ca_2P_2O_7$ for the AIC000 sample, and the main phase shifted to $Ca_9Fe(PO_4)_7$ with the increase of the iron content. The compositions and unit cell parameters were calculated by Rietveld refinement of XRD data and are shown in **Table S2**.The fracture surfaces of the ceramics were examined through SEM (**Figure 6**c-f). The ceramics with AIC000 and AIC004 as the starting materials showed many micro and nano pores on the surface (**Figure 6**c and d), while ceramics using AIC010 and AIC020 as starting materials showed more dense fracture surfaces (**Figure 6**e and f). The acid resistance of the ceramics is evaluated (**Figure S10 and S11)**. The surface morphologies after the acid attack are shown in **Figure S10**. For the samples without or with low amount of iron, the surfaces were severely damaged (**Figure S10**a and b). Meanwhile, for the samples with high iron contents, the surfaces were much smoother (**Figure S10**c and d). The acid resistance of the ceramics was further estimated by the amounts of Ca and P dissolved from the samples. The AIC010 and ACI020 ceramic samples showed much lower amounts of dissolved Ca and P, in comparison with AIC000 and AIC004 ceramic samples, indicating improved acid resistance of the ceramics in the presence of iron. Overall, the ceramics with higher amount of iron exhibited superior acid resistance, showing its great potential for dental applications.

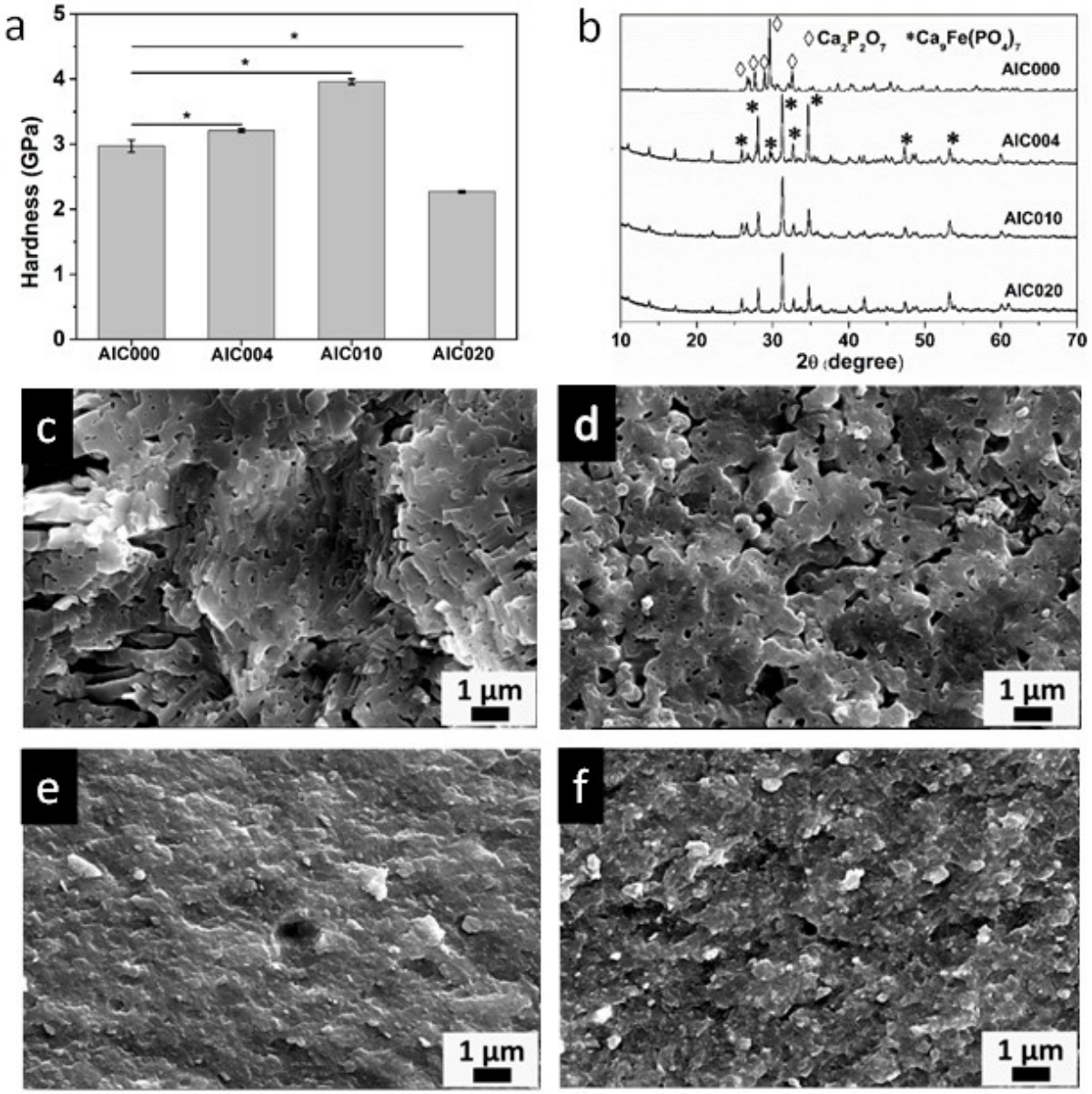

Figure 6. Spark plasma sintered bioceramics using AIC000, AIC004, AIC010, and AIC020 as the raw materials. (a) Hardness and relative density (n=5). (b) XRD pattern. The patterns are matched with the standard diffraction patterns of $Ca_2P_2O_7$ (PDF 00-003-0605) and $Ca_9Fe(PO_4)_7$ (PDF 01-089-0514) (d)-(f) Fracture surface of the ceramics (Magnification x20 000) prepared using AIC000 (c), AIC004 (d), AIC010 (e) and AIC020 (f) as starting materials.

3. Conclusion

Fe-ACP particles with variable content of iron are prepared in the presence of ammonium iron citrate. The Fe-ACP particles are highly stable in aqueous media such as water, SBF and acetate buffer solutions, and their stability in water and in SBF solution depends on the amount of ammonium iron citrate. The Fe-ACP particles show good biocompatibility and osteogenic properties in vitro, and can be applied as starting materials to fabricate calcium phosphate ceramics. With the presence of a proper amount of ammonium iron citrate, ceramics with a hardness higher than human tooth enamel and superior acid resistance can be prepared. The work highlights a novel route to prepare Fe-ACP particles, and presents the potential role of Fe-ACP in biomineralization and as starting material to fabricate acid-resistant high-performance bioceramics.

4. Materials and Methods

4.1. Chemicals

$Ca(NO_3)_2{\cdot}4H_2O$ was purchased from Chinasun Specialty Products Co., Ltd; $Na_2HPO_4{\cdot}12H_2O$ were obtained from Shanghai Lingfeng Chemical Reagent Co., LTD; ammonium iron (III) citrate was purchased from Sigma-Aldrich; ethanol was purchased from Sinopharm Chemical Reagent Co. All chemicals were used as received without further purification. All of the chemicals were of analytical grade. Deionized water was used in all experiments.

4.2. Preparation of Fe-ACP

In a typical experiment, solution 1 was prepared by dissolving 0.3 M $Na_2HPO_4{\cdot}12H_2O$ and a certain amount of ammonium iron (III) citrate (0 M, 0.007 M, 0.02 M, 0.04 M, 0.10 M, 0.20 M) in deionized water. Solution 2 was prepared by dissolving 0.5 M $Ca(NO_3)_2{\cdot}4H_2O$ in deionized water. Solution 2 was slowly added into solution 1 under vigorous stirring at room temperature for 5 minutes. The pH during the synthesis was measured using a pH meter (PB-10, Sartorius). Each experiment has been repeated for three times. The pH electrodes were calibrated by 50 mM $C_8H_5KO_4$ (pH = 4.01, 25 °C), 25 mM NaH_2PO_4/Na_2HPO_4 standard buffer solution (pH = 6.86, 25 °C) and 10 mM $Na_2B_4O_7{\cdot}10H_2O$ standard buffer solution (pH = 9.18, 25 °C). When preparing Fe-ACP particles under pH 4, the pH was adjusted using hydrochloric acid. The particles were separated from the solvent by centrifugation and washed with deionized water three times. Finally, Fe-ACP was washed with ethanol and dried in a vacuum desiccator. The samples were designated as AIC000 (no AIC), AIC0007 (0.007 M AIC), AIC002 (0.02 M

AIC), AIC004 (0.04 M AIC), AIC010 (0.10 M AIC) and AIC020 (0.20 M AIC), according to the concentration of ammonium iron (III) citrate used for the preparation. When preparing particles without citrates, ferric nitrate (0.04 M, 0.10 M) was used instead of ammonium iron (III) citrate. When preparing particles without iron ions, solution 1 was prepared by dissolving 0.3 M $Na_2HPO_4{\cdot}12H_2O$ and a certain amount of citric acid (0.04 M, 0.10 M) in deionized water. The pH of solution 1 was adjusted to the same pH as when ammonium iron citrate（0.04M, 0.10M） were added. Solution 2 was prepared by dissolving 0.5 M $Ca(NO_3)_2{\cdot}4H_2O$ in deionized water, other procedures were similar as mentioned above. When investigating the thermal stability of the particles under different temperatures, the AIC particles were calcined at a predetermined temperature using a muffle furnace (KSL-1700X, Kejing, China). The temperature of muffle furnace rose to the specified temperature at a rate of 10 °C/min, then keeps the specified temperature for 3 hours.

4.3. Preparation of SBF and acetate buffer solutions

The SBF solution was prepared by dissolving NaCl, $NaHCO_3$, KCl, $K_2HPO_4{\cdot}3H_2O$, $MgCl_2{\cdot}6H_2O$, $CaCl_2$ and Na_2SO_4 in de-ionized water, adjusting the ion concentrations to be similar to those in human blood plasma (**Table 1**)[46]. The SBF was buffered at a pH value of 7.40 using $(CH_2OH)_3CNH_2$ and 1.0 M HCl. The acetate buffer solution was prepared by dissolving 1.86 g sodium acetate (0.02269 mol) and 4.64 g acetic acid (0.07731 mol) in 1 L deionized water (pH 4).

Table 1. Ion concentrations of the simulated body fluid and human blood plasma.

Ion	Concentration (mM)	
	Simulated body fluid (SBF)	Human blood plasma
Na^+	142.0	142.0
K^+	5.0	5.0
Mg^{2+}	1.5	1.5
Ca^{2+}	2.5	2.5
Cl^-	147.8	103.0
HCO_3^-	4.2	27.0
HPO_4^{2-}	1.0	1.0
SO_4^{2-}	0.5	0.5

4.4. The stability of Fe-ACP in water, SBF solution and acetate buffer solution

Stability in water and SBF solution: 100 mg freshly prepared Fe-ACP was placed in wide-mouth bottles containing 100 mL deionized water or simulated body fluid (SBF). Afterwards, they were kept in an oscillating incubator at constant temperature (90 rpm, 37.5 °C), respectively. After the predetermined time, the samples were isolated by centrifugation, washed with deionized water and ethanol, and dried in a vacuum desiccator. Stability in acetate buffer solution: 10 mg Fe-ACP particles were put into the beaker with 10 mL acetate buffer solution and intensively stirred. After 15 and 60 min, the solution was filtered with 0.22 μm pore-sized filter and the filtrate was used to measure the ion concentration. Each experiment has been repeated for four times (n=4).

4.5. Scanning electron microscopy (SEM)

The morphology of dried Fe-ACP samples was observed using a scanning electron microscope (S-400, Hitachi, Japan). Specimen were sputtered with a thin Au coating for 45 s before measurement. The samples were mounted on aluminum stubs with double-sided carbon tape. The acceleration voltage was set to 15 kV.

4.6. Transmission electron microscopy (TEM)

A JEOL 2200FS HRTEM operated at 200 kV, equipped with a JEOL EDX detector, was used to perform high-angle annular-dark-field (HAADF) scanning TEM (STEM), and the EDX element line scanning profile as well as the mapping. When preparing samples, the particles were dispersed in ethanol and a drop of the colloidal solution was dipped on a copper grid and then air-dried.

4.7. X-ray powder diffraction (XRD)

Dried Fe-ACP specimen were ground into fine powder and analyzed using an X-ray diffractometer (XRD, Bruker D8 Advance, Germany) equipped with a copper-source, operating at 40 kV and 40 mA. Data were collected for 2θ ranging between 10° and 80° under CuKα radiation (λ = 1.5418). The step size was 0.02° and the residence time was 0.1 s. Qualitative and quantitative phase analyses of the studied samples were conducted on an MDI Jade software. The external standard method and the whole pattern fitting refinement were utilized to obtain the lattice parameters of the studied phases.

4.8. Infrared spectroscopy (FT-IR)

Fourier transform infrared spectroscopy (FT-IR) was performed on a VERTEX 70+HYPERION 2000. The spectra (400-4000 cm^{-1}) were obtained at a resolution of 4 cm^{-1}, using an average signal of 64 scans.

4.9. Thermogravimetric analysis (TGA)

Thermogravimetric analysis (TGA) measurements were performed using a thermal analyzer instrument (SDT Q600, American) under air atmosphere. The samples were heated from ambient temperature to 800 °C at a heating rate equal to 10 °C/min. For each experiment, approximately 2 mg of powdered samples were placed in the crucible of the thermobalance.

4.10. Hardness measurement of sintered ceramics

A micro hardness tester (HVS-1000, Lerot Test Instruments Co., LTD, Shandong, China) was used to measure the Vickers hardness of spark plasma sintered bioceramics on the micro scale with an indentation load of 2.94 N. Five indentations on each sample were conducted and the average values were reported.

4.11. Biocompatibility assessment

The Fe-ACP nanoparticles with different concentrations were prepared using α-MEM medium (Gibco, America) containing 1% streptomycin-penicillin and 10% fetal bovine serum (FBS) (Gibco, America). BMSCs were cultured at a density of 2 ×10^3 cells/well using α-MEM medium for 1, 3, 5 days. At a predetermined time, the CCK-8 assay (Beyotime, China) was performed to evaluate the biocompatibility of Fe-ACP nanoparticles (n=6).

4.12. Alkaline phosphatase (ALP) staining

BMSCs were cultured with different concentrations of AIC010 particles, which were dispersed in an osteogenic induction medium (1% penicillin-streptomycin solution, α-MEM containing 10% FBS, 100 mmol/L of β-glycerophosphate, 2 mmol/L ascorbic acid and 1 μmol/L of dexamethasone) for 7 days. Next, cells were fixed with 4% paraformaldehyde (PFA) and stained using an ALP staining kit (Solarbio, China).

4.13. Alizarin red staining (ARS)

After osteogenic induction of BMSCs which were co-cultured with different concentrations of AIC010 nanoparticles for 14 days, cells were fixed with 4% PFA and stained with an Alizarin Red solution (Solarbio, China) for 30 min. The images were obtained using an optical microscope.

4.14. Spark plasma sintering (SPS)

Spark plasma sintering (Labox 325, Sinter Land, Japan) was utilized to consolidate the raw powder. Approximately 0.5 g powder was loaded in a graphite die (with a diameter of 10 mm) and two graphite punch units. A low pressure (approximately 10 MPa) was applied to the die to pre-press the powder. At the beginning of the sintering experiment, the pressure of the chamber was evacuated to lower than 20 Pa. The instrument took 2 minutes to warm up from room temperature to 570 ºC. After that, the powder was heated up from 570 ºC to the highest sintering temperature (900 ºC) with a ramping rate of 50 ºC/min. The dwell time at 900 ºC was 5 minutes. The temperature was monitored by a thermocouple inserted into a non-through hole of the graphite die. An uniaxial pressure was applied gradually at the punch unit, reaching a maximum of 40 MPa before the temperature reached 700 ºC, and the pressure was maintained during the entire sintering process. The residual graphite on the sintered samples was removed by grinding and polishing with SiC paper.

4.15. Acid resistance

The acid resistance of spark plasma sintered ceramics was evaluated in a citric acid buffer solution (10 mM). The citric acid buffer solution (pH=5) was prepared by adding citric acid monohydrate (10 mM) and trisodium citrate dihydrate (10 mM) into deionized water. The Fe-ACP sintered ceramic was immersed in 10 mL citric acid buffer solution at 37 ℃After 72 hours, the citric acid buffer solution was filtered with 0.22 μm pore-sized filter and the filtrate was used to measure the ion concentrations. The surface of the ceramics after acid resistance assay was analyzed by SEM. The solution was collected for ion release measurement. Ion concentrations were measured by inductively coupled plasma atomic emission spectroscopy (SPECTRO Analytical Instrument, Agilent 7800, America), measuring atomic Ca at 393.366 nm, P at 177.495 nm, and Fe at 259.940 nm.

4.16. Statistical analysis

Quantitative data were expressed as the mean ± standard deviation. One-way analysis of variance (ANOVA) followed by Tukey post hoc comparison (OriginLab Corporation, MA, USA) was used for statistical analysis. A value of $p < 0.05$ denotes a statistically significant difference.

Supporting Information

Supporting Information is available from the Wiley Online Library or from the authors.

Acknowledgements

This work was supported by National Natural Science Foundation of China (82002275, 32271421, 81925027), the Natural Science Foundation of the Jiangsu Higher Education Institutions of China (20KJB430041), and the Priority Academic Program Development of Jiangsu Higher Education Institutions.

Author contributions

Conceptualization: S.C., H.C., B.L. Methodology: S.C., H.C., B.L. Investigation: S.C., D.L., L.F., B.N., Z.C., B.W. Visualization: S.C., D.L., L.F. Discussion of data and useful suggestions: J.K., E.V.S, H.J.H., H.Y., H.C., B.L. Writing-original draft: S.C., D.L. Writing-review and editing: S.C., L.F, H.C., B.L.

Competing interests

The authors declare that they have no competing interests.

Data and materials availability

All data needed to evaluate the conclusions in the paper are present in the paper and/or the Supplementary Materials.

References

[1] a) L. C. Chow, S. Takagi, G. L. Vogel, *J Dent Res* **1998**, 76, 1433; b) H. A. Lowenstam, *Science* **1981**, 211, 1126; c) S. Boonrungsiman, E. Gentleman, R. Carzaniga, N. D. Evans, D. W. McComb, A. E. Porter, M. M. Stevens, *P Natl Acad Sci USA* **2012**, 109, 14170; d) F. Nudelman, K. Pieterse,

A. George, P. H. H. Bomans, H. Friedrich, L. J. Brylka, P. A. J. Hilbers, G. de With, N. A. J. M. Sommerdijk, *Nat Mater* **2010**, 9, 1004; e) A. Lotsari, A. K. Rajasekharan, M. Halvarsson, M. Andersson, *Nature Communications* **2018**, 9, 4170.

[2] a) C. Combes, C. Rey, *Acta Biomater* **2010**, 6, 3362; b) B.-Q. Lu, N. A. Garcia, D. M. Chevrier, P. Zhang, P. Raiteri, J. D. Gale, D. Gebauer, *Cryst Growth Des* **2019**, 19, 3030.

[3] a) D. D. Pei, J. L. Sun, C. H. Zhu, F. C. Tian, K. Jiao, M. R. Anderson, C. Yiu, C. Huang, C. X. Jin, B. E. Bergeron, J. H. Chen, F. R. Tay, L. N. Niu, *Adv Sci* **2018**, 5, 1800873; b) T. Iwayama, T. Okada, T. Ueda, K. Tomita, S. Matsumoto, M. Takedachi, S. Wakisaka, T. Noda, T. Ogura, T. Okano, P. Fratzl, T. Ogura, S. Murakami, *Science Advances* **2019**, 5.

[4] a) M. J. Olszta, D. J. Odom, E. P. Douglas, L. B. Gower, *Connect Tissue Res* **2003**, 44 326; b) S. Weiner, *Bone* **2006**, 39, 431; c) J. Mahamid, A. Sharir, L. Addadi, S. Weiner, *P Natl Acad Sci USA* **2008**, 105, 12748; d) A. La Fontaine, A. Zavgorodniy, H. W. Liu, R. K. Zheng, M. Swain, J. Cairney, *Science Advances* **2016**, 2, e1601145; e) S. Sviben, A. Gal, M. A. Hood, L. Bertinetti, Y. Politi, M. Bennet, P. Krishnamoorthy, A. Schertel, R. Wirth, A. Sorrentino, E. Pereiro, D. Faivre, A. Scheffel, *Nature Communications* **2016**, 7, 11228; f) A. Dey, P. H. H. Bomans, F. A. Muller, J. Will, P. M. Frederik, G. de With, N. A. J. M. Sommerdijk, *Nat Mater* **2010**, 9, 1010.

[5] a) H. A. Lowenstam, S. Weiner, *Science* **1985**, 227, 51; b) J. Mahamid, B. Aichmayer, E. Shimoni, R. Ziblat, C. Li, S. Siegel, O. Paris, P. Fratzl, S. Weiner, L. Addadi, *Proc Natl Acad Sci U S A* **2010**, 107, 6316; c) W. J. E. M. Habraken, J. H. Tao, L. J. Brylka, H. Friedrich, L. Bertinetti, A. S. Schenk, A. Verch, V. Dmitrovic, P. H. H. Bomans, P. M. Frederik, J. Laven, P. van der Schoot, B. Aichmayer, G. de With, J. J. DeYoreo, N. A. J. M. Sommerdijk, *Nature Communications* **2013**, 4, 1507.

[6] a) C. Bussola Tovani, A. Gloter, T. Azaïs, M. Selmane, A. P. Ramos, N. Nassif, *Acta Biomaterialia* **2019**, 92, 315; b) D. Lee, P. N. Kumta, *Mat Sci Eng C-Mater* **2010**, 30, 1313; c) X. Jing, Q. Ding, Q. Wu, W. Su, K. Yu, Y. Su, B. Ye, Q. Gao, T. Sun, X. Guo, Xj, Ts, Xg, Xj, Xj, Qd, Ws, Ky, Xj, Qd, Ws, Ky, Ys, By, Qw, Qg, Ts, Xj, Qd, Ws, Ky, Xj, Xj, Qd, Ws, Ky, Xj, Qd, Ws, Ky, Ys, Xg, *Biomater Transl* **2021**, 2, 197; d) J. Li, F. Cao, B. Wu, J. Yang, W. Xu, W. Wang, X. Wei, G. Liu, D. Zhao, *J Orthop Translat* **2021**, 30, 82; e) A. La Fontaine, A. Zavgorodniy, H. Liu, R. Zheng, M. Swain, J. Cairney, *Sci Adv* **2016**, 2, e1601145.

[7] M. I. Siponen, P. Legrand, M. Widdrat, S. R. Jones, W. J. Zhang, M. C. Y. Chang, D. Faivre, P. Arnoux, D. Pignol, *Nature* **2013**, 502, 681.

[8] a) D. Faivre, T. U. Godec, *Angew Chem Int Edit* **2015**, 54, 4728; b) J. Knaus, *Doctoral dissertation* Doctoral thesis, University of Konstanz. http://nbn-resolving.de/urn:nbn:de:bsz:352-2-nvnnnzvzmd6j3, **2019**.

[9] V. Srot, B. Bussmann, U. Salzberger, J. Deuschle, M. Watanabe, B. Pokorny, I. J. Turinek, A. F. Mark, P. A. van Aken, *Acs Nano* **2017**, 11, 239.

[10] L. M. Gordon, M. J. Cohen, K. W. MacRenaris, J. D. Pasteris, T. Seda, D. Joester, *Science* **2015**, 347, 746.

[11] a) W. Pon-On, N. Charoenphandhu, J. Teerapornpuntakit, J. Thongbunchoo, N. Krishnamra, I. M. Tang, *Mater Chem Phys* **2013**, 141, 850; b) Q. Chang, D. L. Chen, H. Q. Ru, X. Y. Yue, L. Yu, C. P. Zhang, *Biomaterials* **2010**, 31, 1493; c) S. Gomes, A. Kaur, J. M. Greneche, J. M. Nedelec, G. Renaudin, *Acta Biomaterialia* **2017**, 50, 78; d) H. S. Shi, F. P. He, J. D. Ye, *J Mater Chem B* **2016**, 4, 1712.

[12] F. Soetaert, P. Korangath, D. Serantes, S. Fiering, R. Ivkov, *Adv Drug Deliver Rev* **2020**, 163, 65.

[13] a) L. L. Sheng, Z. W. B. Zhang, Y. Zhang, E. D. Wang, B. Ma, Q. Xu, L. L. Ma, M. Zhang, G. Pei, J. Chang, *Biomaterials* **2021**, 264; b) I. Ullah, W. C. Zhang, L. Yang, M. W. Ullah, O. M. Atta, S. Khan, B. Wu, T. J. Wu, X. L. Zhang, *Mat Sci Eng C-Mater* **2020**, 110.

[14] L. G. Ding, H. Wang, J. Y. Li, D. C. Liu, J. Z. Bai, Z. Q. Yuan, J. J. Yang, L. Bian, X. J. Zhao, B. Li, S. Chen, *Biomater Sci-Uk* **2022**, 11, 96.

[15] a) S. H. Maxian, J. P. Zawadsky, M. G. Dunn, *J Biomed Mater Res* **1993**, 27, 111; b) R. B. Heimann, R. Wirth, *Biomaterials* **2006**, 27, 823; c) M. Nagano, T. Nakamura, T. Kokubo, M. Tanahashi, M. Ogawa, *Biomaterials* **1996**, 17, 1771; d) J. Knaus, D. Schaffarczyk, H. Colfen, *Macromol Biosci* **2020**, 20; e) Y. Li, Q. Pan, J. Xu, X. He, H. A. Li, D. A. Oldridge, G. Li, L. Qin, *J Orthop Translat* **2021**, 27, 110; f) Y. H. Z. Feng, D. Wu, J. Knaus, S. Kessler, B. Ni, Z. K. Chen, J. Avaro, R. Xiong, H. Coelfen, Z. L. Wang, *Adv Healthc Mater* **2023**, DOI: 10.1002/adhm.202203411.

[16] a) C. Qi, Y. J. Zhu, X. Y. Zhao, B. Q. Lu, Q. L. Tang, J. Zhao, F. Chen, *Chemistry* **2013**, 19, 981; b) G. J. Ding, Y. J. Zhu, C. Qi, B. Q. Lu, J. Wu, F. Chen, *J Colloid Interface Sci* **2015**, 443, 72.

[17] a) A. D. Van Staden, L. M. Dicks, *J Appl Biomater Funct Mater* **2012**, 10, 2; b) T. Yu, J. Ye, Y. Wang, *J Biomed Mater Res B Appl Biomater* **2009**, 90, 745; c) E. Steijvers, A. Ghei, Z. Xia, Zx, Zx, Es, Ag, Zx, Ag, *Biomater Transl* **2022**, 3, 65.

[18] a) Y. B. Li, W. J. Weng, *J Mater Sci-Mater M* **2007**, 18, 2303; b) B. H. Fellah, P. Layrolle, *Acta Biomaterialia* **2009**, 5, 735; c) T. Yu, J. D. Ye, Y. J. Wang, *J Biomed Mater Res B* **2009**, 90b, 745; d) S. Segman-Magidovich, H. Grisaru, T. Gitli, Y. Levi-Kalisman, H. Rapaport, *Adv Mater* **2008**, 20, 2156.

[19] M. J. Olszta, X. G. Cheng, S. S. Jee, R. Kumar, Y. Y. Kim, M. J. Kaufman, E. P. Douglas, L. B. Gower, *Mat Sci Eng R* **2007**, 58, 77.

[20] L. B. Gower, D. J. Odom, *J Cryst Growth* **2000**, 210, 719.

[21] L. N. Niu, S. E. Jee, K. Jiao, L. Tonggu, M. Li, L. Wang, Y. D. Yang, J. H. Bian, L. Breschi, S. S. Jang, J. H. Chen, D. H. Pashley, F. R. Tay, *Nat Mater* **2017**, 16, 370.

[22] Z. M. Liu, C. Y. Shao, B. Jin, Z. S. Zhang, Y. Q. Zhao, X. R. Xu, R. K. Tang, *Nature* **2019**, 574, 394.

[23] a) Y. Y. Hu, A. Rawal, K. Schmidt-Rohr, *P Natl Acad Sci USA* **2010**, 107, 22425; b) E. Davies, K. H. Muller, W. C. Wong, C. J. Pickard, D. G. Reid, J. N. Skepper, M. J. Duer, *P Natl Acad Sci USA* **2014**, 111, E1354; c) Y. Wang, S. Von Euw, F. M. Fernandes, S. Cassaignon, M. Selmane, G. Laurent, G. Pehau-Arnaudet, C. Coelho, L. Bonhomme-Coury, M. M. Giraud-Guille, F. Babonneau, T. Azais, N. Nassif, *Nat Mater* **2013**, 12, 1144.

[24] A. L. Boskey, A. S. Posner, *J Phys Chem* **1973**, 77, 2313.

[25] C. Holt, M. J. J. M. Vankemenade, L. S. Nelson, D. W. L. Hukins, R. T. Bailey, J. E. Harries, S. S. Hasnain, P. L. Debruyn, *Mater Res Bull* **1989**, 24, 55.

[26] A. Akiva, M. Kerschnitzki, I. Pinkas, W. Wagermaier, K. Yaniv, P. Fratzl, L. Addadi, S. Weiner, *J Am Chem Soc* **2016**, 138, 14481.

[27] E. R. Kramer, A. M. Morey, M. Staruch, S. L. Suib, M. Jain, J. I. Budnick, M. Wei, *J Mater Sci* **2013**, 48, 665.

[28] J. Vecstaudza, M. Gasik, J. Locs, *J Eur Ceram Soc* **2019**, 39, 1642.

[29] F. Tamimi, Z. Sheikh, J. Barralet, *Acta Biomaterialia* **2012**, 8, 474.

[30] a) S. Chen, K. Grandfield, S. Yu, H. Engqvist, W. Xia, *Crystengcomm* **2016**, 18, 1064; b) S. Chen, M. Krumova, H. Colfen, E. V. Sturm, *Chem Mater* **2019**, 31, 1543.

[31] a) F. J. Martinez-Casado, M. Iafisco, J. M. Delgado-Lopez, C. Martinez-Benito, C. Ruiz-Perez, D. Colangelo, F. Oltolina, M. Prat, J. Gomez-Morales, *Crystal Growth & Design* **2016**, 16, 145; b) C. Santos, M. M. Almeida, M. E. Costa, *Crystal Growth & Design* **2015**, 15, 4417; c) Y. Chen, W. J. Gu, H. H. Pan, S. Q. Jiang, R. K. Tang, *Crystengcomm* **2014**, 16, 1864; d) W. G. Jiang, H. H. Pan, Y. R. Cai, J. H. Tao, P. Liu, X. R. Xu, R. K. Tang, *Langmuir* **2008**, 24, 12446.

[32] C. Y. Shao, R. B. Zhao, S. Q. Jiang, S. S. Yao, Z. F. Wu, B. Jin, Y. L. Yang, H. H. Pan, R. K. Tang, *Adv Mater* **2018**, 30, 1704876.

[33] A. Hirsch, I. Azuri, L. Addadi, S. Weiner, K. S. Yang, S. Curtarolo, L. Kronik, *Chem Mater* **2014**, 26, 2934.

[34] L. D. Esposti, A. Adamiano, A. Tampieri, G. B. Ramirez-Rodriguez, D. Siliqi, C. Giannini, P. Ivanchenko, G. Martra, F. H. Lin, J. M. Delgado-Lopez, M. Iafisco, *Crystal Growth & Design* **2020**, 20, 3163.

[35] S. Weiner, I. Sagi, L. Addadi, *Science* **2005**, 309, 1027.

[36] a) A. Lotsari, A. K. Rajasekharan, M. Halvarsson, M. Andersson, *Nat Commun* **2018**, 9; b) S. Ucar, S. H. Bjornoy, D. C. Bassett, B. L. Strand, P. Sikorski, J. P. Andreassen, *Cryst Growth Des* **2019**, 19, 7077.

[37] A. L. Boskey, A. S. Posner, *J Phys Chem* **1973**, 77, 2313.

[38] M. Schweikle, S. H. Bjornoy, A. T. J. van Helvoort, H. J. Haugen, P. Sikorski, H. Tiainen, *Acta Biomaterialia* **2019**, 90, 132.

[39] N. C. Blumenthal, F. Betts, A. S. Posner, *Calc Tiss Res* **1977**, 23, 245.

[40] C. B. Tovani, A. Gloter, T. Azais, M. Selmane, A. P. Ramos, N. Nassif, *Acta Biomaterialia* **2019**, 92, 315.

[41] M. Iafisco, G. B. Ramirez-Rodriguez, Y. Sakhno, A. Tampieri, G. Martra, J. Gomez-Morales, J. M. Delgado-Lopez, *Crystengcomm* **2015**, 17, 507.

[42] E. Ruiz-Agudo, C. Ruiz-Agudo, F. Di Lorenzo, P. Alvarez-Lloret, A. Ibanez-Velasco, C. Rodriguez-Navarro, *Acs Biomater Sci Eng* **2021**, 7, 2346.

[43] H. D. Kim, S. Amirthalingam, S. L. Kim, S. S. Lee, J. Rangasamy, N. S. Hwang, *Adv Healthc Mater* **2017**, 6, 1700612.

[44] M. A. Saghiri, A. Asatourian, J. Orangi, C. M. Sorenson, N. Sheibani, *Crit Rev Oncol Hemat* **2015**, 96, 129.
[45] H. H. K. Xu, D. T. Smith, S. Jahanmir, E. Romberg, J. R. Kelly, V. P. Thompson, E. D. Rekow, *J Dent Res* **1998**, 77, 472.
[46] T. Kokubo, H. Takadama, *Biomaterials* **2006**, 27, 2907.

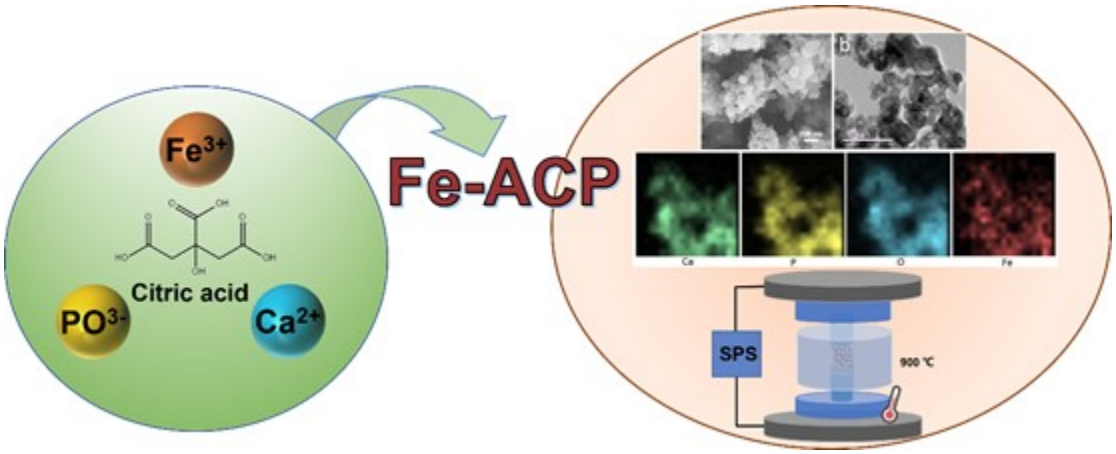

An iron-bearing amorphous calcium phosphate (Fe-ACP) is prepared in the presence of ammonium iron citrate. The Fe-ACP particles can be highly stable in water and simulated body fluid. The particles show good biocompatibility and osteogenic properties. By applying the Fe-ACP particles as initial powders, calcium iron phosphate ceramics with superior mechanical strength and acid resistance are prepared.